Published for SISSA by Springer

Received: October 25, 2020
Accepted: October 29, 2020
Published: December 7, 2020

JHEP12(2020)042

Erratum: NNLO QCD corrections to jet production in deep inelastic scattering

James Currie,[a] **Thomas Gehrmann,**[b] **Alexander Huss**[c] **and Jan Niehues**[b]

[a] *nstitute for Particle Physics Phenomenology, Durham University, South Road, Durham, DH1 3LE, U.K.*

[b] *Department of Physics, Universität Zürich, Winterthurerstrasse 190, CH-8057 Zürich, Switzerland*

[c] *Institute for Theoretical Physics, ETH, Wolfgang-Pauli-Strasse 27, CH-8093 Zürich, Switzerland*

E-mail: james.currie@durham.ac.uk, thomas.gehrmann@uzh.ch, ahuss@itp.phys.ethz.ch, jan@physik.uzh.ch

Erratum to: JHEP07(2017)018

Abstract: We correct an error in the implementation of specific integrated initial-final antenna functions that impact the numerical predictions for the DIS process.

ArXiv ePrint: 1703.05977

https://doi.org/10.1007/JHEP12(2020)042

Contents

1 Introduction **1**

4 Inclusive jet production **1**
- 4.1 Structure of the inclusive jet production cross section at NNLO 1
- 4.2 Comparison to HERA data 1

5 Di-jet production **4**
- 5.1 Scale setting in the di-jet production cross section at NNLO 4
- 5.2 Comparison to HERA data 4

6 Summary and conclusion **10**

JHEP12(2020)042

1 Introduction

We computed the NNLO QCD corrections to the DIS process for inclusive single jet production and di-jet production in the Breit frame in [1]. In the context of performing consistency checks using integrated antenna functions, we have uncovered an error in the numerical implementation for some of these functions associated with the initial-final configuration. While this error was found to have no impact on hadron-collider processes owing to specific pairings of terms that mutually compensate the error, this is not the case for the DIS process. We have therefore recomputed all numerical results presented in [1]. In addition, we have included corrections factors for the ZEUS dijet measurement (figures 8–12) that were provided with the measurement but not included previously.

Numbering of sections and figures is as in [1].

4 Inclusive jet production

The setup of the calculation is described in detail in [1].[1] The kinematic selection follows the H1 [2, 3] and ZEUS measurements [4, 5].

4.1 Structure of the inclusive jet production cross section at NNLO

The relative contribution of the quark- and gluon-induced channels is shown in figure 3 and a breakdown into different exclusive jet multiplicities is given in figure 4.

4.2 Comparison to HERA data

A comparison between NNLO predictions and the data for inclusive jet production is shown in figure 5 and 6 for the H1 and ZEUS measurements, respectively. The NNLO corrections are smaller compared to the results in [1] and exhibit an improved perturbative convergence with the NNLO curve always lying within the scale uncertainty band of the previous order.

[1] We note that there is a typo in the summary of the fiducial cuts for the ZEUS measurement given in table 6 of [1]: Instead of $-1.0 < \eta^B < 2$, it should instead read $-1.5 < \eta^B < 2$.

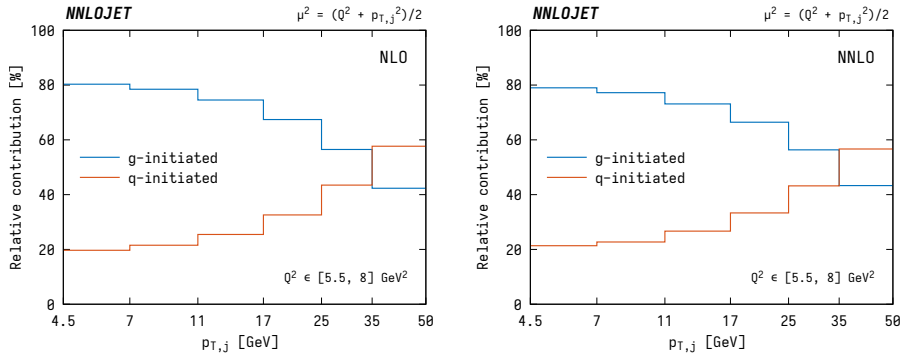

Figure 3. Quark- and gluon-initiated contributions to the inclusive jet transverse momentum distribution at NLO and NNLO.

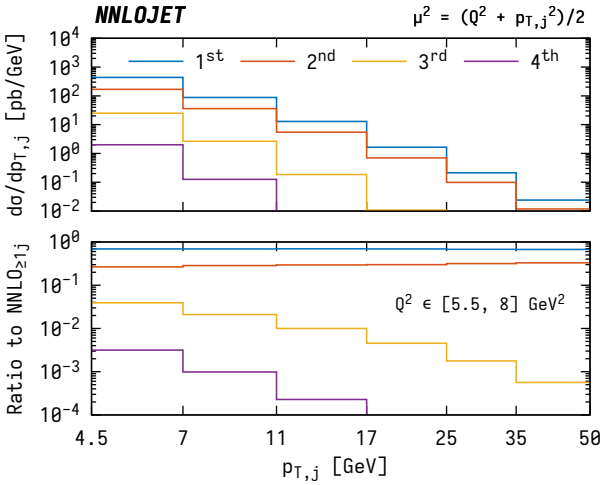

Figure 4. Contributions to inclusive jet production (k_T-algorithm with $R_0 = 1$) from first, second, third, and fourth jet.

JHEP12(2020)042

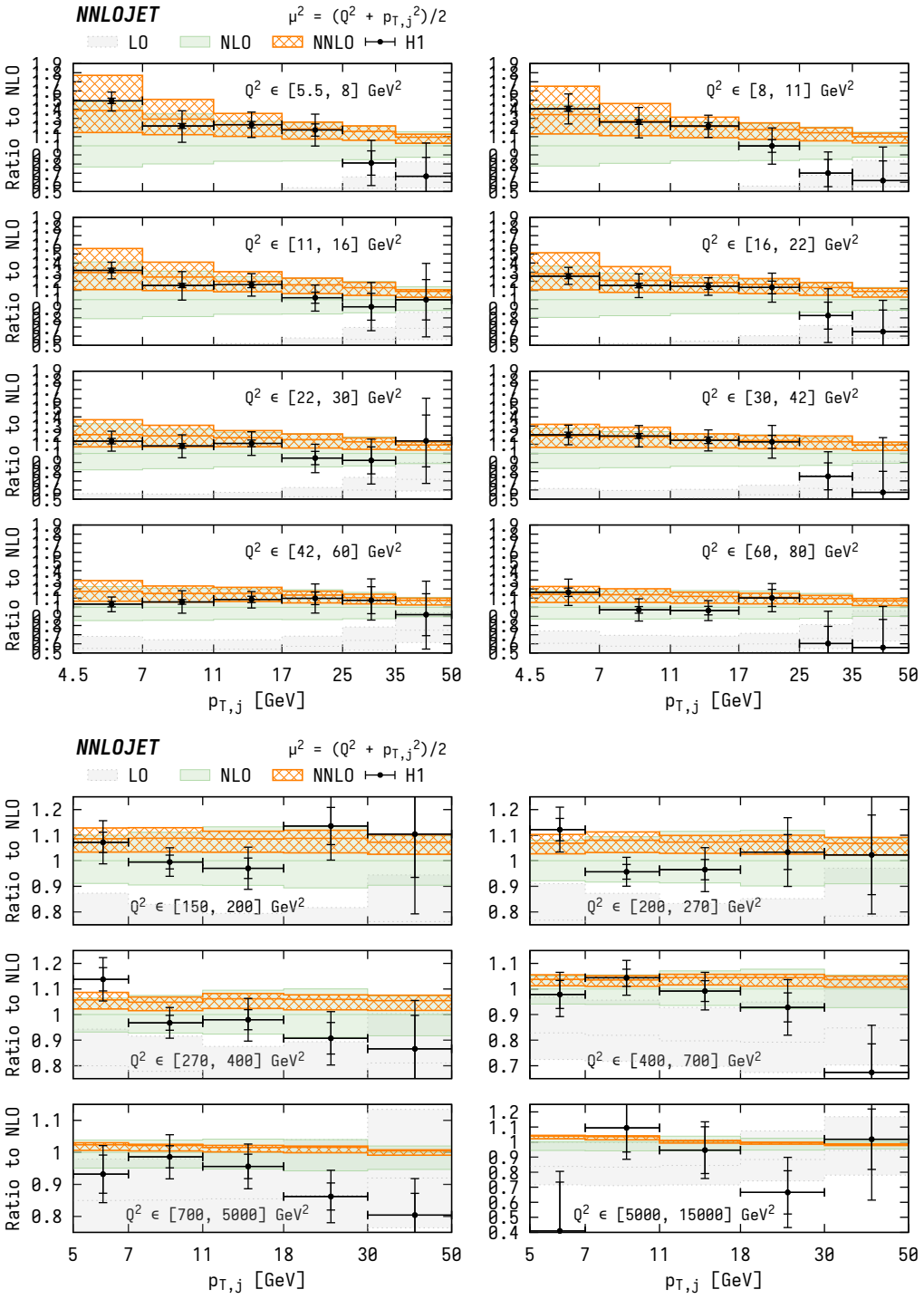

Figure 5. Inclusive jet production cross section as a function of the jet transverse momentum $p_{T,B}$ in bins of Q^2, compared to H1 data.

JHEP12(2020)042

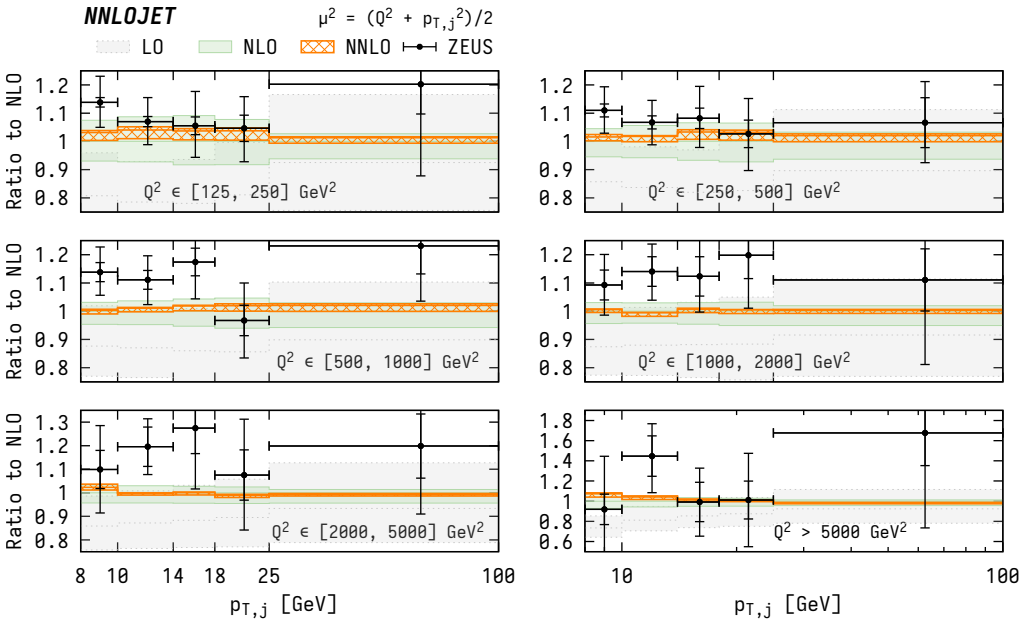

Figure 6. Inclusive jet production cross section as a function of the jet transverse momentum $p_{T,B}$ in bins of Q^2, compared to ZEUS data.

5 Di-jet production

The setup of the calculation is described in detail in [1]. The kinematic selection follows the H1 [2, 3] and ZEUS measurements [6].

5.1 Scale setting in the di-jet production cross section at NNLO

A study of different choices for the central scales is presented in figure 7, where we compare the following three options:

$$\begin{aligned}
&\text{(a)} \quad \mu_f^2 = \mu_r^2 = \left(Q^2 + \langle p_T^B \rangle_2^2\right)/2, \\
&\text{(b)} \quad \mu_f^2 = Q^2, \quad \mu_r^2 = \left(Q^2 + \langle p_T^B \rangle_2^2\right)/2, \\
&\text{(c)} \quad \mu_f^2 = \mu_r^2 = Q^2.
\end{aligned}$$

5.2 Comparison to HERA data

A comparison between NNLO predictions and the ZEUS data for di-jet production [6] is shown in figures 8–12. In addition to correcting the error in the antenna function, we now also include the correction factors accounting for hadronisation effects and the Z-boson exchange denoted as "$C_{\text{hadr}} \cdot C_{Z^0}$" in [6], which were not included previously.

Figure 8 displays the inclusive di-jet cross section for the ZEUS kinematics as a function of the electron variables Q^2 (left) and of x (right). We observe the NNLO corrections to be sizeable especially at low values of Q^2 or x, where they enhance the NLO prediction by about 10%. In this region, the scale dependence of the NNLO prediction is as large as at NLO, or even larger. We note that the data is better described by the NNLO prediction

JHEP12(2020)042

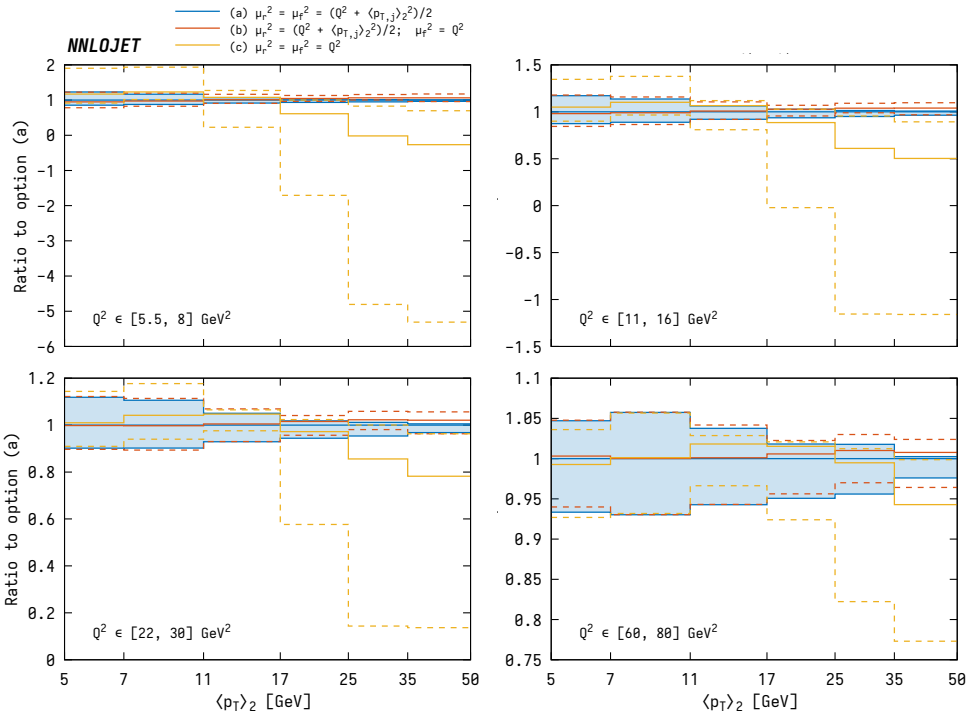

Figure 7. Di-jet production cross sections for different scale settings.

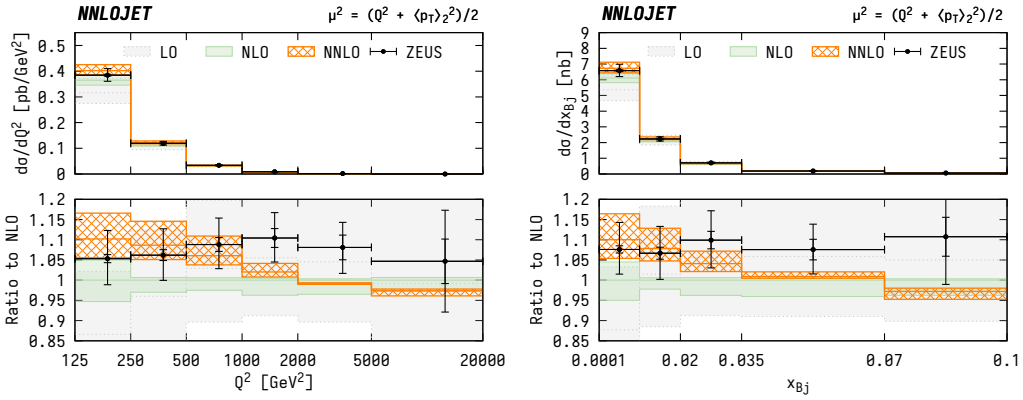

Figure 8. Inclusive di-jet production cross section as a function of the electron variables Q^2 (left) and x (right), compared to ZEUS data.

than at NLO. A similar pattern is observed in the distributions in $\langle p_T^B\rangle_2$ and M_{jj} shown in figure 9, with sizeable NNLO corrections in the lower range of the distributions.

The di-jet cross section as function of η^* and of $\log(\xi_2)$ is shown in figure 11. While good perturbative convergence is observed in the plateau region $\eta^* < 0.65$, NNLO corrections turn out to be very sizeable at higher rapidities. The perturbative instability in this region was already pointed out and explained by the ZEUS collaboration [6]. Even so, going from NLO to NNLO we observe a much improved description of the data in this region. The

JHEP12(2020)042

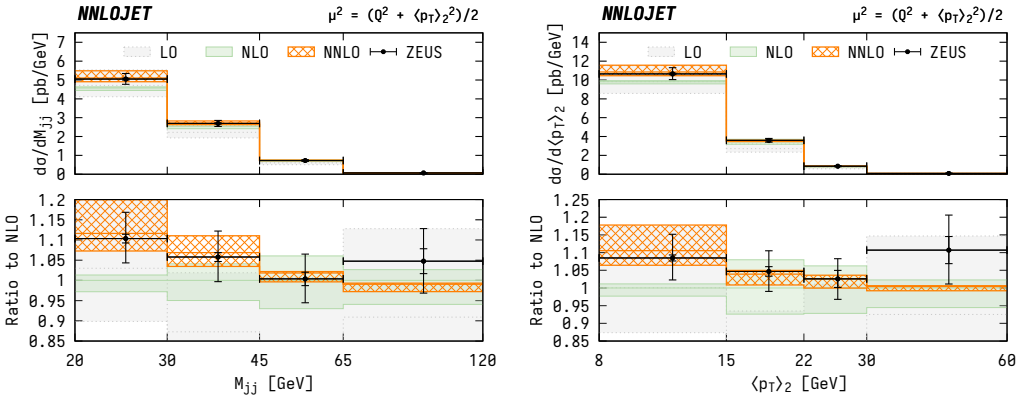

Figure 9. Inclusive di-jet production cross section as a function of $\langle p_T^B \rangle_2$ (left) and M_{jj} (right), compared to ZEUS data.

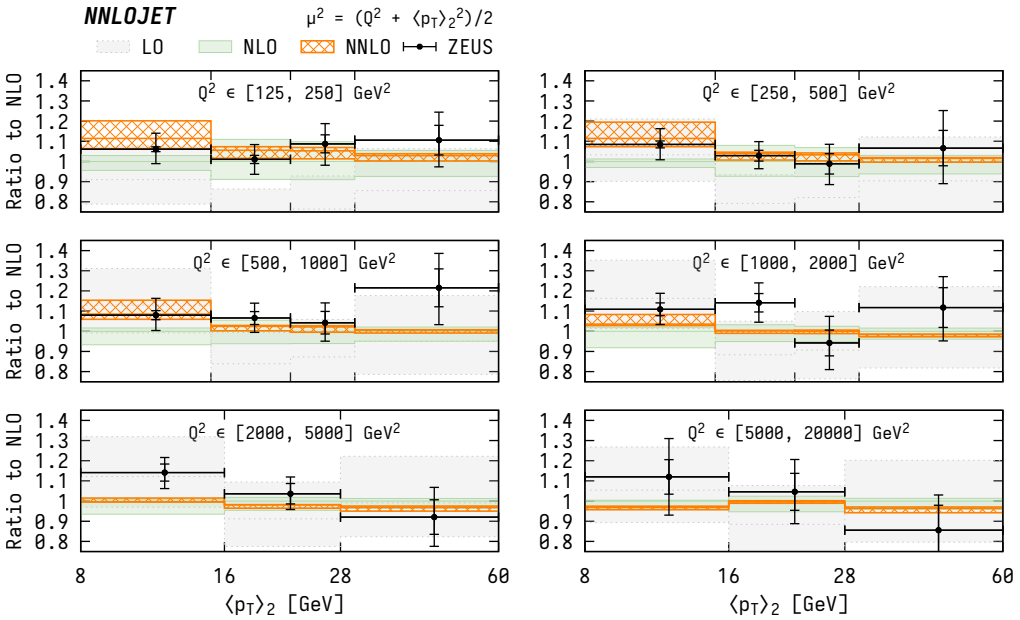

Figure 10. Inclusive di-jet production cross section as a function of $\langle p_T^B \rangle_2$ in bins of Q^2, compared to ZEUS data.

$\log(\xi_2)$ correlates most directly with the parton distributions, indicating the importance of NNLO corrections in describing the data at momentum fractions in the medium range $0.01 < \xi < 0.1$. The double-differential distribution in $\log(\xi_2)$ and Q^2, figure 12, further illustrates this impact, showing a coherent pattern of sizeable NNLO corrections that are crucial in describing the data both in normalisation and shape over the full Q^2 range.

A comparison between NNLO predictions and the H1 data for di-jet production [2, 3] is shown in figures 13–15.

The potential perturbative instabilities that may arise from the symmetric cuts on p_T^B combined with a cut on M_{jj} is studied in figure 16 by contrasting the results of figure 15

JHEP12(2020)042

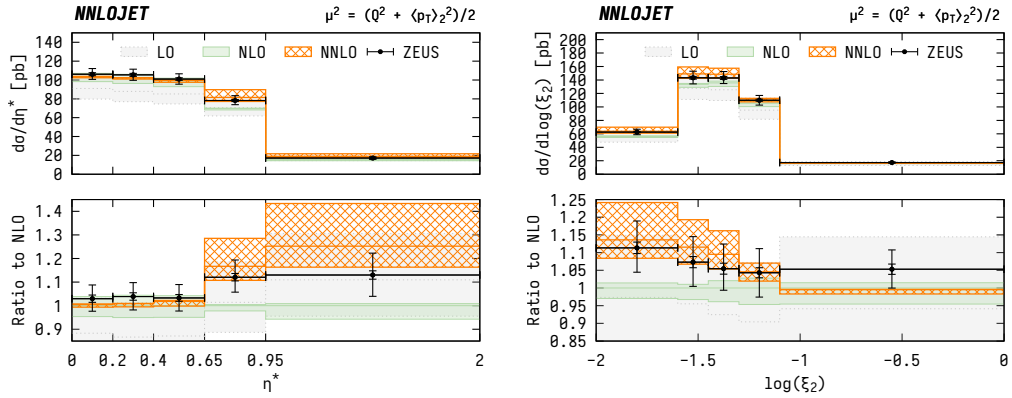

Figure 11. Inclusive di-jet production cross section as a function of η^* (left) and $\log(\xi_2)$ (right), compared to ZEUS data.

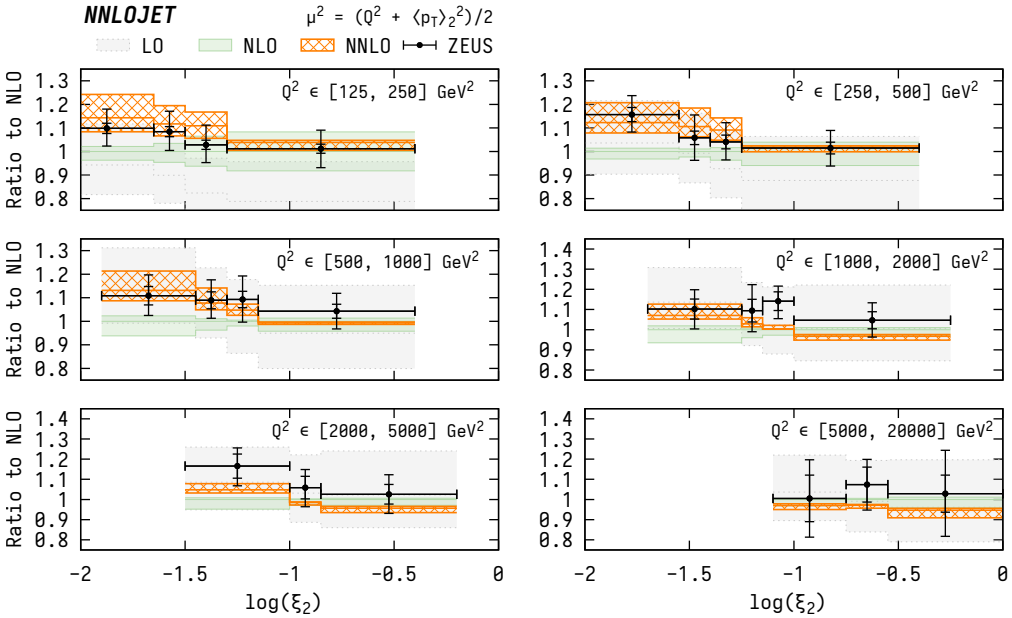

Figure 12. Inclusive di-jet production cross section as a function of $\log(\xi)$ in bins of Q^2, compared to ZEUS data.

with a calculation using different set of jet cuts: $p^B_{T,j1} > 5\,\text{GeV}$, $p^B_{T,j2} > 4\,\text{GeV}$. We observe a very substantial improvement in the perturbative convergence, compared to the cuts used in the H1 analysis [2].

JHEP12(2020)042

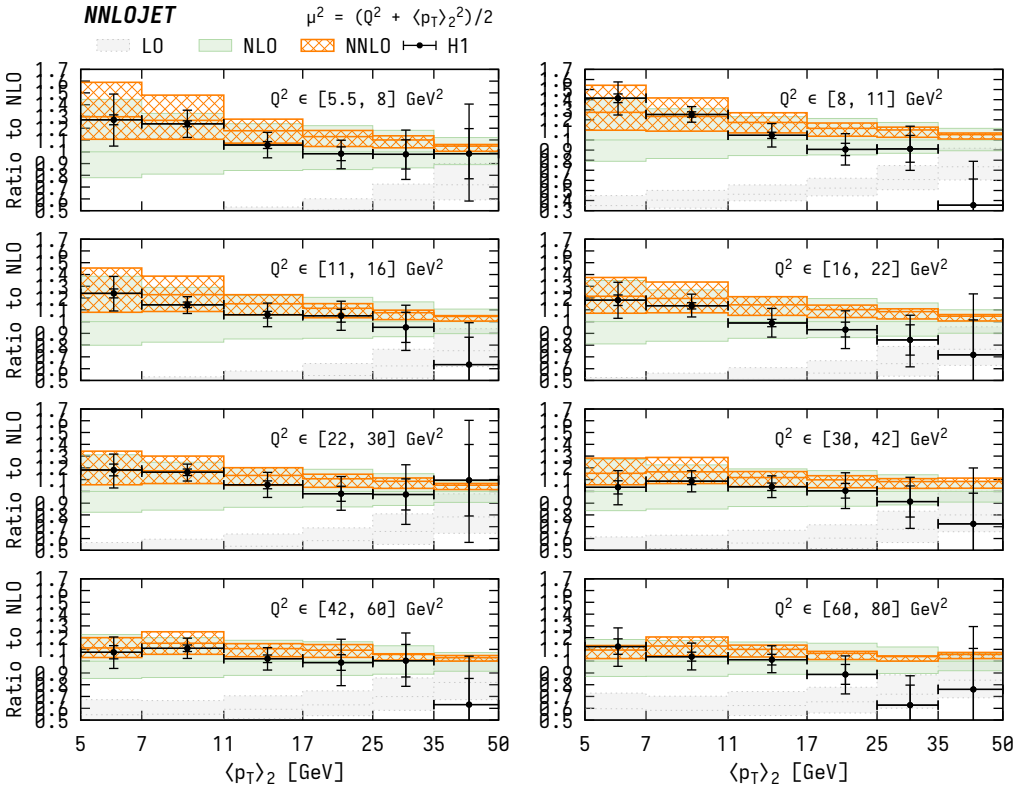

Figure 13. Inclusive di-jet production cross section as a function of $\langle p_T^B \rangle_2$ in bins of Q^2, compared to H1 low-Q^2 data.

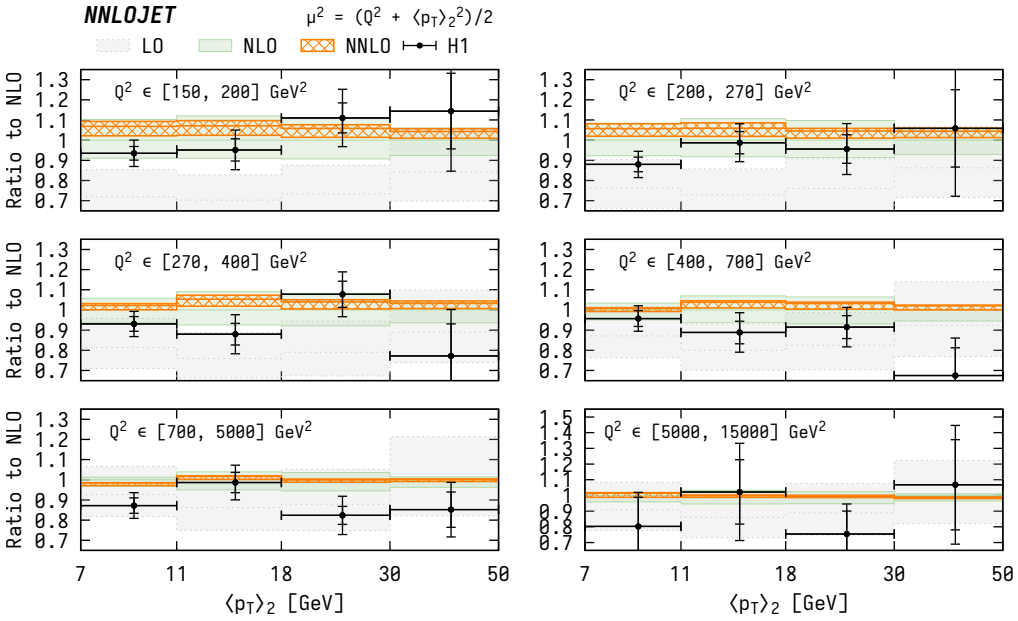

Figure 14. Inclusive di-jet production cross section as a function of $p_{T,2}^B$ in bins of Q^2, compared to H1 high-Q^2 data.

JHEP12(2020)042

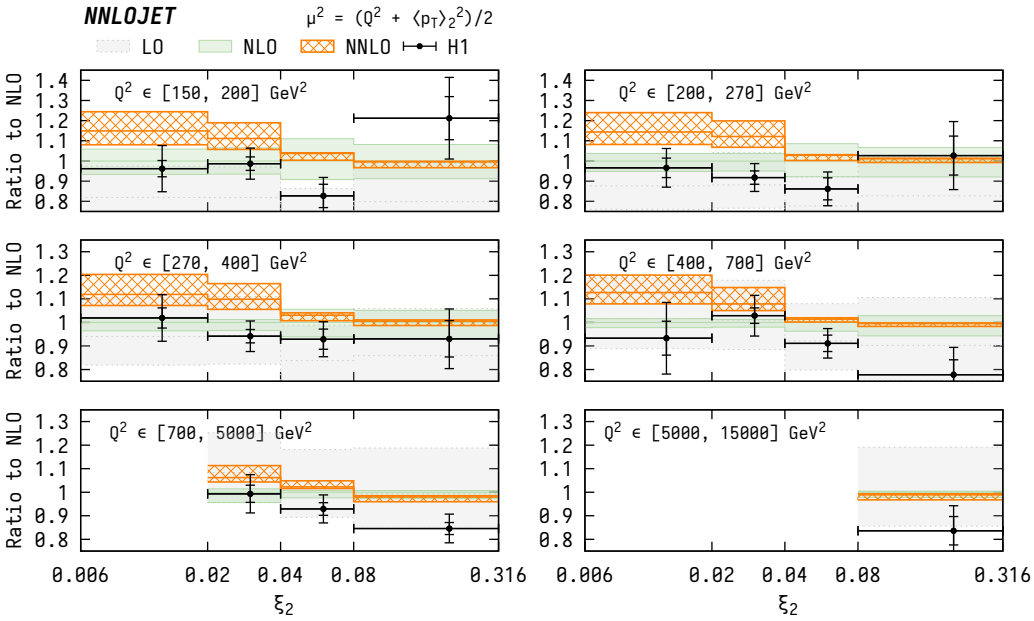

Figure 15. Inclusive di-jet production cross section as a function of ξ_2 in bins of Q^2, compared to H1 high-Q^2 data.

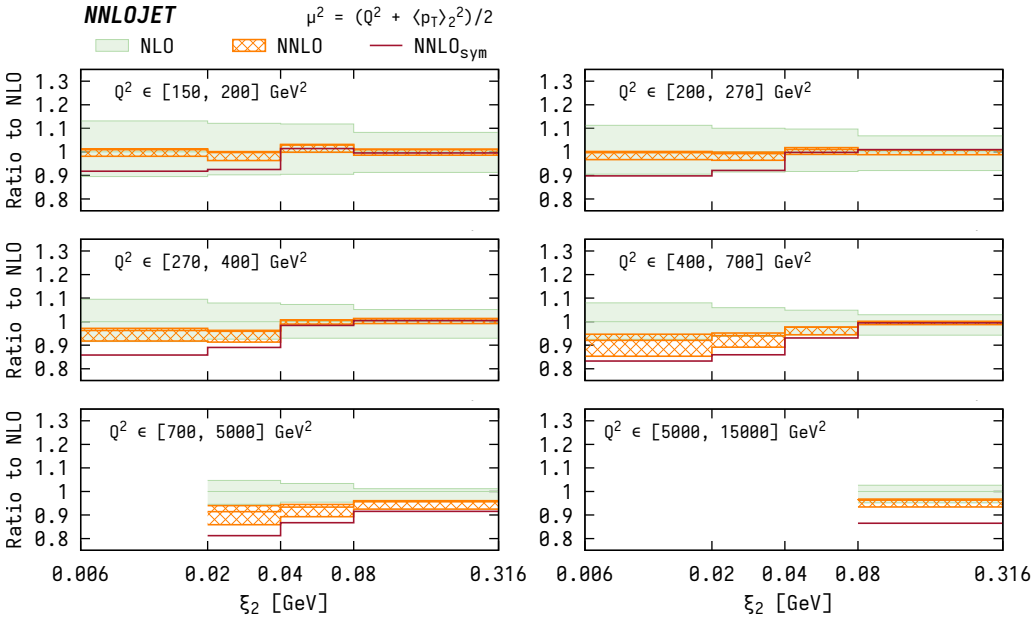

Figure 16. Inclusive di-jet production cross section as a function of ξ_2 in bins of Q^2 with asymmetric cuts on the two jets. The red line indicates the NNLO prediction with symmetric cuts of figure 15.

JHEP12(2020)042

6 Summary and conclusion

In this erratum, we have corrected an implementation error in the calculation of NNLO corrections to the DIS process computed in [1]. We have updated all our results and observe a quite sizeable impact resulting from this error. The NNLO corrections are typically found to be smaller in magnitude compared to the results presented in [1]. As a result, the perturbative convergence is often visibly improved with NNLO prediction typically falling within the uncertainty estimates at NLO. Most striking differences are observed in observables and kinematic regions that are particularly sensitive to infrared physics and where higher-order corrections are very substrantial. Here we observe a very much improved agreement between our predictions and the measurements.

Acknowledgments

We thank Robin Schürmann for performing independent re-derivations of integrated initial-final antenna functions, which have led us to uncover the implementation error that is corrected in this erratum.

References

[1] J. Currie, T. Gehrmann, A. Huss and J. Niehues, *NNLO QCD corrections to jet production in deep inelastic scattering*, *JHEP* **07** (2017) 018 [arXiv:1703.05977] [INSPIRE].

[2] H1 collaboration, *Measurement of multijet production in ep collisions at high Q^2 and determination of the strong coupling α_s*, *Eur. Phys. J. C* **75** (2015) 65 [arXiv:1406.4709] [INSPIRE].

[3] H1 collaboration, *Measurement of Jet Production Cross Sections in Deep-inelastic ep Scattering at HERA*, *Eur. Phys. J. C* **77** (2017) 215 [arXiv:1611.03421] [INSPIRE].

[4] ZEUS collaboration, *Jet-radius dependence of inclusive-jet cross-sections in deep inelastic scattering at HERA*, *Phys. Lett. B* **649** (2007) 12 [hep-ex/0701039] [INSPIRE].

[5] ZEUS collaboration, *Inclusive-jet cross sections in NC DIS at HERA and a comparison of the kT, anti-kT and SIScone jet algorithms*, *Phys. Lett. B* **691** (2010) 127 [arXiv:1003.2923] [INSPIRE].

[6] ZEUS collaboration, *Inclusive dijet cross sections in neutral current deep inelastic scattering at HERA*, *Eur. Phys. J. C* **70** (2010) 965 [arXiv:1010.6167] [INSPIRE].

JHEP12(2020)042